What Determines the Sign Reversal of Magnetoresistance in a Molecular Tunnel Junction?

Subhasish Mandal and Ranjit Pati*

Department of Physics, Michigan Technological University, Houghton, Michigan 49931, United States

ABSTRACT

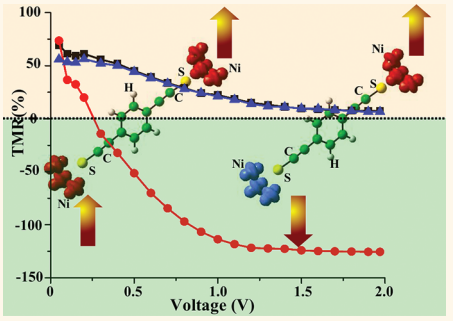

The observations of both positive and negative signs in tunneling magnetoresistance (TMR) for the same organic spin-valve structure have baffled researchers working in organic spintronics. In this article, we provide an answer to this puzzle by exploring the role of metal—molecule interface on TMR in a single molecular spin-valve junction. A planar organic molecule sandwiched between two nickel electrodes is used to build a prototypical spin-valve junction. A parameter-free, single-particle Green's function approach in conjunction with a posteriori, spin-unrestricted density functional theory involving a hybrid orbital-dependent functional is used to calculate the spin-polarized current. The effect of external bias is explicitly included to investigate the spin-valve behavior. Our calculations show that only a small change in the interfacial distance at the metal—molecule junction can alter the sign of the TMR from a positive to a negative value. By changing the interfacial distance by 3%, the number of participating eigenchannels as well as their orbital characteristics changes for the antiparallel configuration, leading to the sign reversal in TMR.

KEYWORDS: electronic structure · molecular tunnel junction · density functional theory · spin-dependent transport · single-particle Green's function · magnetoresistance · spin-valve

A series of successful measurements of electron transport in molecular junctions in recent years have inspired researchers to look for ways to exploit the quantum spin state of the electron with intriguing possibilities of realizing a new paradigm in molecular scale electronics.[1−5] Typically, the spin relaxation time in an organic molecule, which bridges two magnetic electrodes, is longer than the time-of-flight of the electrons from one electrode to the other electrode. In addition, the chemical flexibility, low-cost production, as well as the lack of spin−orbit and hyperfine coupling in small organic molecules leading to a longer spin-coherence length make them ideal candidates for exploring coherent spin-conserved tunneling. Though spin transport in an organic molecular spin-valve junction has been studied extensively,[6−12] several fundamental questions remain elusive. For example, researchers have reported a positive sign[6] for the magnetoresistance in contrast to a negative sign reported by other groups in the same organic spin-valve structure.[9−11]

In an organic spin-valve device structure, where two ferromagnetic electrodes are separated by an insulating or semiconducting organic layer, the resistance of the circuit depends upon the direction of magnetization at the electrodes. Usually, the device resistance changes from minimal resistance for parallel magnetization (PC) to maximal for antiparallel magnetization (APC) between the contacts. This gives a positive sign in the magnetoresistance. The negative sign in magnetoresistance arises when the device resistance in the case of parallel magnetization is higher than that obtained with the antiparallel magnetization between the electrodes. Using a tris(8-hydroxyquinoline)aluminum (Alq3) organic spacer between two ferromagnetic electrodes, several groups[9−11] detected a negative sign in magnetoresistance in contrast to the positive magnetoresistance reported by Barraud *et al.*[6] in the same spin-valve structure. These controversial findings have baffled researchers working in this field.[13,14] The origin of such anomalous behavior lies in the incomplete understanding of the electronic structure details at the metal—molecule interface as well as the spin-polarized electronic structure of the spacer including the effect of bias. Considering the

* Address correspondence to patir@mtu.edu.

Received for review February 13, 2012 and accepted March 12, 2012.

Published online March 12, 2012
10.1021/nn3006569

true quantum nature of the problem involving spin state of the electron, first principles theoretical methods are necessary to address this problem. However, only a few foremost first principles works on spin transport in a single molecular spin-valve junction have been reported.[15−20] In all of these works, the spin-valve actions were demonstrated only at zero bias or at a very small bias range (∼mV) or using zero-bias spectra—leaving an open and challenging question on the efficiency of the spin-valve when a relatively higher external bias is applied. In addition to the broken symmetry wave function due to the opposite alignment of the magnetization at the two electrodes in the antiparallel configuration, how the external bias further affects the magnetic state is a challenging task to probe within the density functional framework.

In this article, we have constructed a prototypical molecular spin-valve device by sandwiching a planar organic molecule 1,4-diethynylbenzene between two nickel electrodes to investigate the bias-dependent spin-valve action. Particularly, we try to answer several questions: What is the reason behind obtaining both positive and negative signs in magnetoresistance for the same spin-valve device structure? How does external bias affect the magnitude as well as the sign of the tunneling magnetoresistance (TMR)? The bias-dependent effects (first and higher order Stark effects) are explicitly incorporated in our model. The calculations are carried out using a first principles spin-polarized, orbital-dependent density functional theory (DFT). A parameter-free, single-particle Green's function approach[14,21−25] is used to calculate the spin-polarized electronic current.

Our calculations reveal that by changing the interfacial distance (d) from its equilibrium value of 2.06 to 2.00 Å (∼3% change), the sign of TMR changes from a positive to a negative value. In the case of d = 2.00 Å, the current in the APC is found to be significantly higher than that in the PC, resulting in a negative sign in TMR. In contrast, a positive TMR is observed for d = 2.06 Å. The large increase in the number of participating eigenstates as well as the change in their orbital character in the APC is found to be responsible for the increase in current. In the APC, the occupied orbitals, which have significant Ni d character, contribute to the spin-polarized current at d = 2.00 Å. On the contrary, at d = 2.06 Å, unoccupied orbitals, which have only Ni s and p character, take part in conduction. This clearly suggests that a small change in interfacial distance, which may be generated by thermal fluctuation in the experimental condition, could lead to a different sign in TMR. Apart from this, we quantitatively present the magnetic proximity effect and its bias-dependent nature, which can be used to understand the unexpected magnetism often observed[26−28] in organic materials that are in close proximity with magnetic substrates. At the same time, this work provides a unique pathway to electrical manipulation of quantum spin state, which would help to understand the newly born spinterface science.

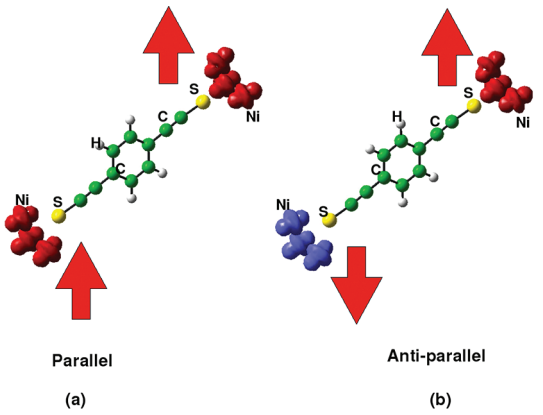

Figure 1. Electron spin density plot for (a) parallel and (b) antiparallel alignment of spins at the two electrodes. Red represents positive (up) spin density, and blue represents negative (down) spin density. Solid arrow represents the direction of magnetization at the electrodes. The atoms in the molecular spacer have much smaller spin density (not visible) compared to the spin density at Ni.

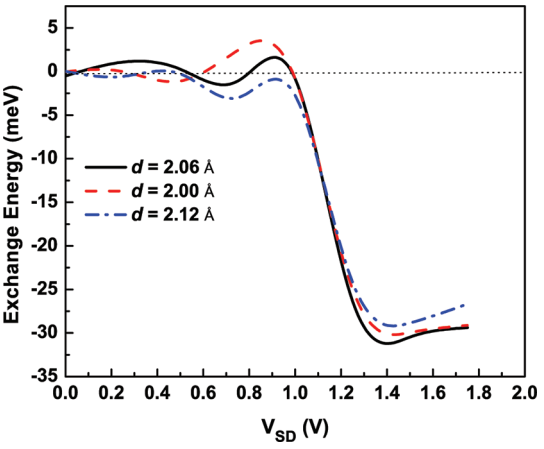

Figure 2. Bias-dependent exchange energy ($E_{PC} - E_{APC}$) for the spin-valve device with three interfacial distances (d).

RESULTS AND DISCUSSION

Spin Density and Energetics. In Figure 1, we present calculated spin densities of the device at equilibrium for both PC and APC. For the parallel spin configuration, the total magnetic moment at each electrode is found to be ∼3 μ_B, while for the APC, it is found to be ∼3 μ_B at one electrode and ∼−3 μ_B at the opposite electrode. It should be noted that the small gain in magnetic moment (maximum ∼0.1 μ_B) by the nonmagnetic molecule compared to the much larger magnetic moment at Ni (∼1 μ_B per atom) is not visible in Figure 1. Next, we calculate the exchange energy (E_{ex}), that is, the energy difference between PC and APC ($E_{PC} - E_{APC}$) of the extended system. At equilibrium (V_{SD} = 0 V), E_{ex} is found to be −0.0299 meV with APC to be lower in energy than PC. This value is comparable to

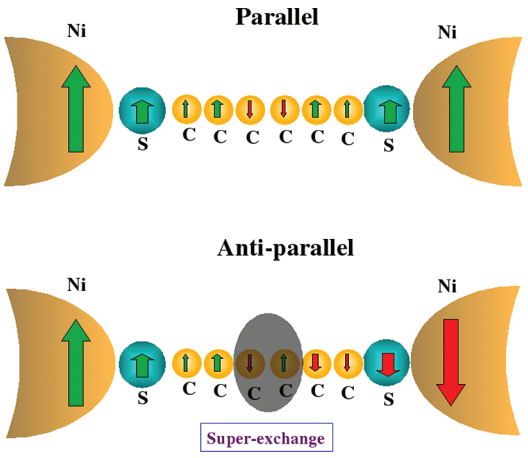

Figure 3. Schematic representation of spin-profile along the wire axis for both the parallel and antiparallel configurations; up (down) arrows refer to the positive (negative) magnetic moment.

the energy difference reported earlier in carbon-based molecular spin-valve junctions.[15,19] The analysis of spin density distribution in the extended molecule for parallel and antiparallel configurations (shown in Figure 3) suggests that the stability of the antiparallel magnetic state is dictated by the super exchange interaction. The bias-dependent E_{ex} for all three interfacial distances are plotted in Figure 2. They all found to exhibit similar behavior in E_{ex} upon applied bias. For a bias range from 0 to ~1 V, the E_{ex} shows a small oscillation. After 1 V, a sudden drop in E_{ex} (~30 meV) is observed. It clearly suggests that the antiparallel configuration becomes more stable after $V_{SD} \sim 1$ V. The enhanced stability of the antiparallel spin state after 1 V can be ascribed to the stronger superexchange interaction caused by the observed equal increase in the magnitude of the magnetic moment at the nickel site. In contrast, in the parallel magnetic configuration, the increase of bias beyond 1 V makes the spin distribution asymmetric at the two electrodes (magnitude of the magnetic moments at two electrodes are slightly different) resulting in a decrease in stability. This study thus confirms the manipulation of spin state at the junction by applied bias—a prerequisite for a spin-engineered device.

Magnetic Proximity. When a metallic lead is coupled with a semiconducting molecule, the metallic property of the lead transfers to the semiconducting molecule. Likewise, when a ferromagnetic lead is in close proximity with a nonmagnetic material, the nonmagnetic material gains some magnetic property due to exchange interaction. This is referred to as magnetic proximity effect,[29] which plays an important role in spin injection. In our spin-valve structure, a ferromagnetic lead is in contact with a nonmagnetic DTB molecule, allowing the molecular spacer to gain some magnetic property due to proximity effect. How the spin distribution in the nonmagnetic molecular spacer,

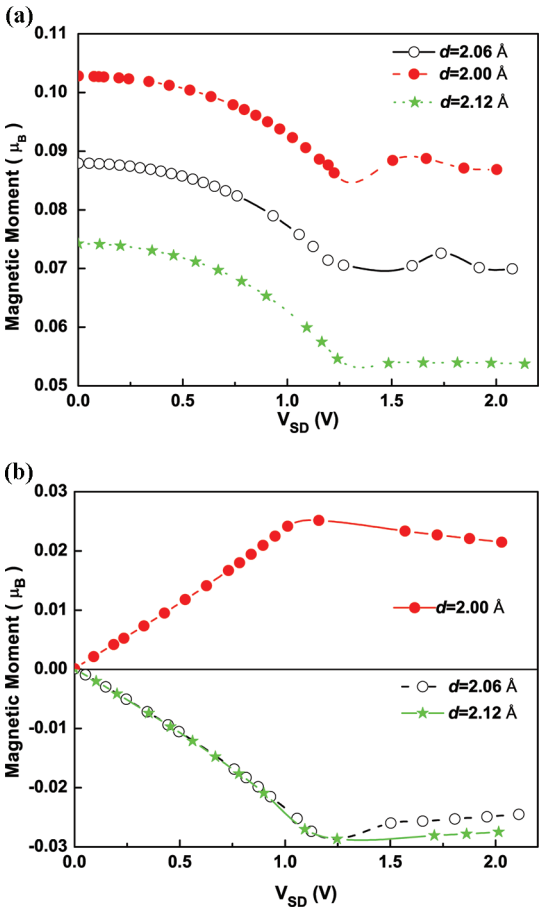

Figure 4. Bias-dependent magnetic moment of the molecular spacer for (a) parallel and (b) antiparallel alignment of spins at two electrodes; *d* refers to the interfacial distance.

for parallel and antiparallel spin configuration at the electrodes, is affected by this proximity effect is a challenging question. The other important questions are as follows: How does the applied bias affect the spin distribution in the nonmagnetic molecular spacer? How does a change in interfacial distance affect the magnetic character of the spacer? To answer these questions, we looked at the bias-dependent acquired magnetic moment of the molecular spacer (M_μ) in parallel and antiparallel configurations for three different interfacial distances. In the parallel configuration (Figure 4a), for all three different *d* values, a similar evolution of M_μ with applied bias is noted. As expected, for a larger *d*, the acquired magnetic moment is found to be smaller. For example, at equilibrium (V_{SD} = 0 V), for *d* = 2.00, 2.06, and 2.12 Å, the M_μ is found to be 0.102, 0.088, and 0.074 μ_B, respectively. It is important to note that, in recent experiments, a magnetic moment of 0.05 μ_B per carbon atom was found in C/Fe multilayered system[27] and in meteorite graphite.[26] On a similar note, the shape of the spin-up d states is reported to be strongly affected by the hybridization with the p state of C atom when an organic molecule adsorbs on the Fe surface.[28] Further inspection of

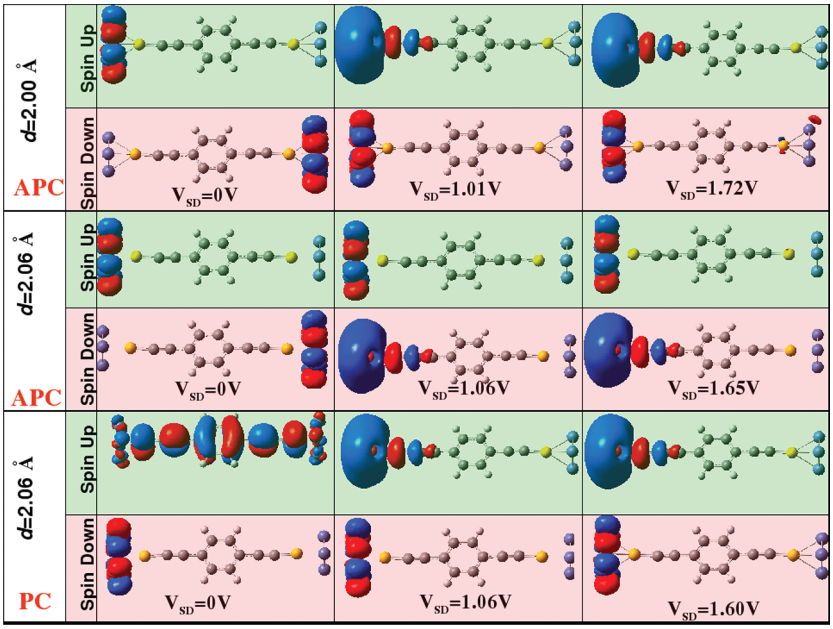

Figure 5. Bias-dependent highest occupied molecular orbital (HOMO) for the extended molecule; green panels show the HOMO for spin-up states, while red panels show that for spin-down states.

Figure 4a reveals that an increase in applied bias from 0 to ~1.2 V results in a decrease in M_μ; a subsequent increase in bias has almost no effect on M_μ.

In the case of APC (Figure 4b), as the magnetic moments at the two electrodes are equal and opposite in sign, there is a zero net gain in magnetic moment of the spacer at equilibrium (Figure 3); the atoms in the vicinity of the Ni electrode having a positive (negative) value of magnetic moment, gain a positive (negative) magnetic moment. For d = 2.06 and 2.12 Å, the M_μ is found to be negative when a finite bias is applied, while for d = 2.00 Å, the acquired magnetic moment is found to be positive. For all interfacial distances, the magnitude of the M_μ steadily increases for a bias range of 0 to ~1.2 V. Analogous to the PC, a further increase in applied bias yields almost no effect on the spacer magnetic moment. The origin of such intriguing behavior can be unraveled by understanding the orbital hybridization at the metal–molecule junction. Since the frontier orbitals dictate the electronic and magnetic properties, we have plotted the highest occupied molecular orbitals for the spin-up and spin-down states in the extended molecule (Figure 5). Several remarks are in order. First, for PC, the strong orbital hybridization between Ni and the spacer molecule is found for the spin-up state at equilibrium, resulting in a positive magnetic moment in the molecular spacer. As the bias is applied, the symmetry of the wave function breaks and the molecular orbital starts to localize in the direction of the electric field; this leads to a decrease in M_μ. Increasing the bias beyond 1.2 V yields almost no change in the strength of the hybridization between Ni and the molecular spacer. This explains the flat nature of the magnetic moment after V_{SD} ~ 1.2 V. It is important to note that, for the PC, the spin-down state does not evolve with the bias. Next, turning to the APC, at equilibrium, the contribution from the spin-up and spin-down states (Figure 5) cancels out, resulting in a net magnetic moment of zero for all three interfacial distances. However, the change in interfacial distance is found to have a significant effect on the bias-dependent orbital evolution. For d = 2.06 Å, the spin-down states evolve with the increase of bias. In contrast, for d = 2.00 Å, the spin-up states evolve. This explains the positive value for M_μ at d = 2.00 Å and the negative value for M_μ at d = 2.06 Å. A closer inspection reveals that the strength of hybridization between Ni and the molecule increases with the increase in bias up to ~1.2 V. This leads to an increase in the magnitude of M_μ with bias. Increasing the bias beyond 1.2 V does not affect the strength of hybridization, and hence M_μ remains almost unchanged.

Current–Voltage. Next, we turn our discussions to current–voltage (I–V) characteristics of the molecular spin-valve device for three different interfacial distances. The current is calculated within the coherent and spin-conserved tunneling limit. The results are summarized in Figure 6. Total current for both PC (I_{PC}) and APC (I_{APC}) is obtained by adding the currents for the spin-up and spin-down states. The contribution to the current from the spin-up and spin-down states is almost identical in the case of APC, while for the PC, the spin-up contribution is higher than that for the spin-down states for all three different d values. A nonlinear feature in I–V is noticeable for all three different d values. From Figure 6, a similar trend in I–V is noted for d = 2.06 and 2.12 Å; the current in the PC is found to be higher than that in the APC. For d = 2.00 Å, the current

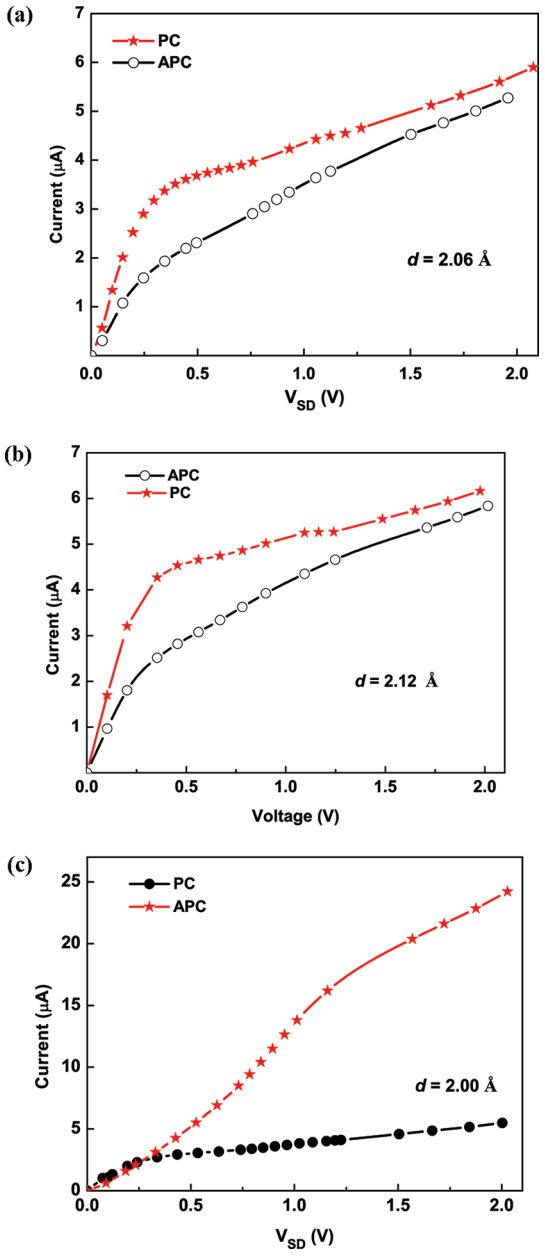

Figure 6. Current−voltage characteristics for the parallel and antiparallel configurations with *d* = (a) 2.06, (b) 2.12, and (c) 2.00 Å.

in PC is found to be higher than that in the APC only for a small bias range of 0 to ~0.25 V; after 0.25 V, with increasing bias, the I_{APC} is found to be significantly higher than that of the I_{PC}. A closer examination reveals that the I_{APC} depends sensitively on the interfacial distance. By changing the *d* from 2.06 to 2.00 Å, the current in the APC is found to increase by ~4 times at ~1 V. In contrast, for the PC, the change in *d* from 2.06 to 2.00 Å yields a decrease in current by 0.86 times.

Tunneling Magnetoresistance. To quantify the spin-valve action in detail, we calculate the TMR as TMR = $(I_{PC} - I_{APC})/((I_{PC} + I_{APC})/2) \times 100\%$. Figure 7 shows TMR as a function of bias voltage for three different interfacial distances. As noted from Figure 6, spin-valve

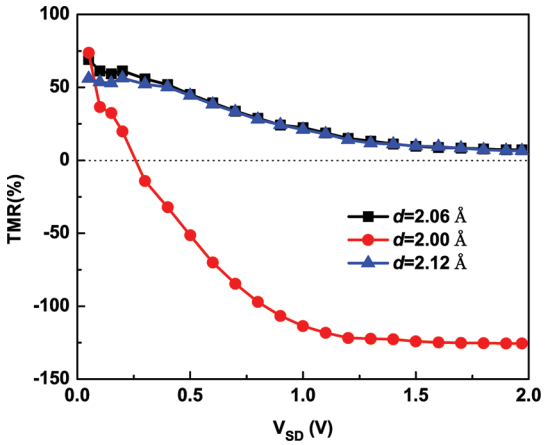

Figure 7. Bias-dependent tunneling magnetoresistance for three interfacial distances (*d*).

structures with *d* = 2.06 and 2.12 Å yield a similar characteristic in TMR; TMR is positive, and the magnitude of TMR is found to decrease with an increase in bias up to 1.25 V and then remains flat. For *d* = 2.00 Å, TMR is found to be positive only for a bias range of 0 to ~0.25 V; a subsequent increase in bias yields a negative TMR which remains flat after $V_{SD} \sim 1.25$ V. For example, at $V_{SD} = 1.00$ V, the TMR for *d* = 2.00 Å is −113.6%, while for *d* = 2.06 Å, the TMR is +22.39%. The similar bias-dependent behavior is also noted in Figure 4, where the acquired magnetic moment of the molecule remains almost flat after $V_{SD} \sim 1.2$ V.

Transmission. To gain deeper insight into the origin of sign reversal in TMR, we calculated spin-polarized bias-dependent transmission for three different interfacial distances. Since both *d* = 2.06 and 2.12 Å show similar trends in TMR, we present spin-polarized transmission for the contrasting cases, that is, for *d* = 2.00 and 2.06 Å in Figure 8. For brevity, we have presented our results at $V_{SD} \sim 1$ V. The dotted lines represent the chemical potential window (CPW). In the case of *d* = 2.06 Å, the spin-up transmission for PC is higher than for APC. This gives a higher net transmission (sum of spin-up and spin-down transmission) in PC than in APC. For example, with *d* = 2.06 Å, at injection energy (*E*) = −0.45 eV, the total transmission for PC is 0.185, while the transmission for APC is 0.150. This explains the observed higher current for PC than APC at *d* = 2.06 Å (Figure 6a), resulting in a positive TMR (Figure 7). Next, we discuss the transmission for *d* = 2.00 Å. We notice that the spin-up and spin-down transmission for the PC is significantly smaller than that for APC. The total transmission at *E* = −0.45 eV for PC is 0.159 and for APC is 0.704. This ~4-fold increase in transmission for APC is attributed to the ~4-fold increase in current at ~1 V for APC (Figure 6c).

Now, a natural question arises: What causes the transmission to behave differently for different *d* values? To understand this, we looked at the eigenchannels that contribute to the transmission within the

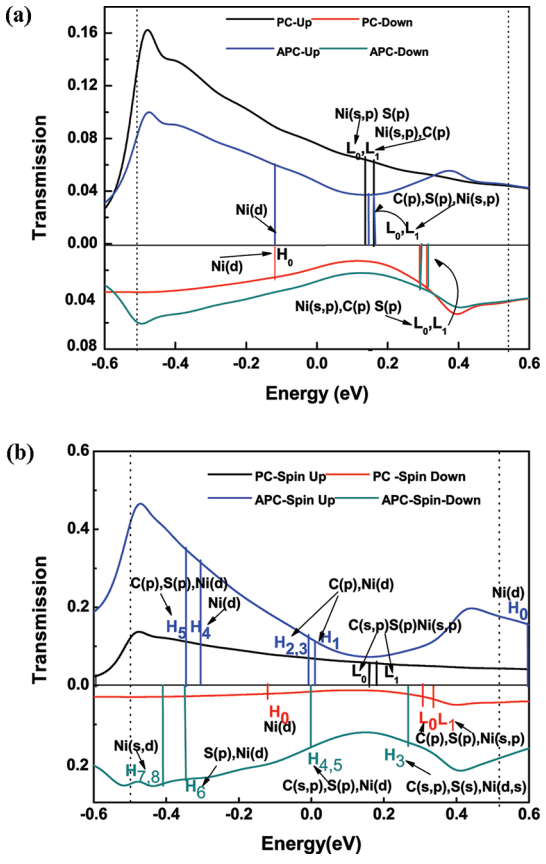

Figure 8. Bias-dependent transmission function for d = (a) 2.06 and (b) 2.00 Å. The Fermi level lies at E = 0. The dotted lines show the chemical potential window. H_0, H_1, H_2, H_3, H_4, H_5, H_6, H_7, H_8 represent HOMO, HOMO-1, HOMO-2, HOMO-3, HOMO-4, HOMO-5, HOMO-6, HOMO-7, and HOMO-8, respectively. L_0 and L_1 represent LUMO and LUMO+1, respectively.

CPW. For APC, the number of eigenchannels within the chemical potential window increases significantly as we change the d from 2.06 to 2.00 Å. For d = 2.06 Å, mainly frontier unoccupied levels having Ni (s,p) characters contribute to the conduction, while for d = 2.00 Å, all of the participating orbitals for APC are found to be occupied with a significant Ni d character. This suggests that a small change in intefacial distance can have a significant effect on the electronic structure of the device, which could lead to the observed sign reversal in TMR.

Molecule–Lead Coupling. Since the conduction in molecular spin-valve junction not only depends on the electronic structure of the molecular spacer but also on the electronic structure at the metal–molecule interface, we looked at the role of molecule–lead coupling on electronic current to discern the junction effect. We recalculated the I_{PC} at 1.0 V for d = 2.00 Å (where the TMR is found to be negative) using C_l^σ and C_r^σ extracted from APC at the same bias. The spin-up current in the PC changes from 2.896 to 3.432 μA, while the spin-down current changes from 0.923 to 7.972 μA; this leads to an increase in total current of ~3 times. Similarly, we recalculated the current for the PC for d = 2.06 Å (where the TMR is found to be positive) using C_l^σ and C_r^σ extracted from the APC at the same bias for the spin-up and spin-down state, respectively. The total current is found to decrease. This clearly reflects that a small change in interfacial distance, which affects the hybridization between Ni and the molecule (shown in Figure 8) and hence the molecule–lead coupling, can have a significant effect on the escape rate of the electrons.

CONCLUSIONS

We have studied spin-polarized transport properties in a prototypical spin-valve junction, which is constructed by sandwiching a 1,4-diethynylbenzene planar organic molecule between two nickel electrodes. A spin-unrestricted, orbital-dependent density functional theory in conjunction with a single-particle Green's function approach is used to calculate the spin-polarized current. Bias effects are explicitly included in our calculations. Our calculation shows that a small change of ~3% in metal–molecule interfacial distance can alter the sign of tunneling magnetoresistance in a molecular spin-valve device. It should be noted that this small change in metal–molecule interfacial distance can be generated by thermal fluctuation. Thus a statistical approach should be adopted in experimental measurement[3] to wash out the uncontrollable interfacial bond-length fluctuation in average spin-polarized conductance, yielding either the positive or negative sign in TMR. Here, the current in the APC is found to be strongly affected by the change in the interfacial distance. The higher current in the APC for certain d is attributed to the increase in the number of eigenchannels with significant Ni d characters. Thus, this work not only provides an explanation for the sign reversal of TMR in a molecular tunnel device at the electronics structure level but it also opens up a new pathway for orbital manipulation in molecular spintronics.

COMPUTATIONAL METHODS

The geometry optimization for the molecule is performed using DFT, which involves Becke's three-parameter hybrid functional (B3LYP) for exchange-correlation. A real-space approach that employs the single determinant many-body wave function is used here. A finite set of Gaussian atomic orbitals[30] is used to construct the wave function. The use of the real-space approach allows us to understand the physical details of the transport process through some important quantities, such as spatial distribution of potential, charge, and spin densities. We have used the all-electron 6-311g basis set to represent the atoms in the DTB. The spin-valve junction is constructed by

sandwiching the DTB between two ferromagnetic Ni electrodes. For the nickel atoms in the electrode, we have used the LANL2DZ basis set that includes the scalar relativistic effects. The thiolate (−S) anchoring group is used to attach the molecule between the electrodes at the most likely three-fold hollow site of the Ni(111) surface. It is important to mention that the charge transport properties through this molecule have been investigated very recently by attaching it between Au electrodes.[31] Since the molecular spacer exchanges its energy and electrons with the semi-infinite electrodes, a rigorous treatment of the device can be achieved by considering it to be an *open* system. To model an open molecular spin-valve junction, we have divided it into two regions. The first one is the active scattering region, which consists of the molecule and a finite number of Ni atoms (three on each side) taken from the Ni(111) surface. The second one is the semi-infinite electrode part, which is assumed to be unperturbed (retain its bulk properties) when the extended molecule is attached to the electrode. During self-consistent calculation, to ensure an extremely tight convergence, the convergence criterion for energy, maximum, and root-mean-square electron density is set at 10^{-10}, 10^{-6}, and 10^{-8} au, respectively. We have constructed a strongly coupled (chemically bonded) junction. The interfacial distance (*d*), which is the distance from the S atom to the vertex of the triangle formed by the three Ni atoms of the Ni(111) surface, is varied for both PC and APC to determine the optimum distance where the repulsive interaction is minimum. For both PC and APC, the optimum distance is found to be 2.06 Å. The energy-distance graph yields a parabolic feature around the optimum distance. Since the metal−molecule interface is the integral part of the device[7,32] that controls the spin transport characteristics, we have considered three different spin-valve structures with *d* of 2.00, 2.06, and 2.12 Å to investigate the junction-dependent TMR. The active scattering region at equilibrium is described by the spin-unrestricted Kohn−Sham DFT that requires the solution of an effective single-particle Schrodinger-like equation

$$H^{\sigma}(0)\psi_i^{\sigma}(\vec{r}) = \left[-\frac{1}{2}\nabla^2 + V_{\text{ion}}(\vec{r}) + \int \mathrm{d}^3\vec{r}\,\frac{\rho(\vec{r})}{|(\vec{r}) - \vec{r}'|} + V_{\text{xc}}^{\sigma} \right] \times \psi_i^{\sigma}(\vec{r}) = E_i^{\sigma}\psi_i^{\sigma}(\vec{r})$$

The terms in the bracket represent electron's kinetic energy, ionic potential, coulomb interaction, and the exchange-correlation potential, respectively. The exchange-correlation potential is expressed in terms of the hybrid functional as: $V_{xc}^{\sigma}(\vec{r}) = (\delta E_{xc}^{\text{B3LYP}}[\rho^{\uparrow},\rho^{\downarrow}])/(\delta\rho^{\sigma})$, where $\sigma = \uparrow,\downarrow$ and $\rho(\vec{r}) = \rho^{\uparrow} + \rho^{\downarrow}$; $\rho^{\sigma} = \sum_i n_i^{\sigma}|\psi\rho_i^{\sigma}(\vec{r})|^2$. Here n_i^{σ} is the occupation number of the spin-dependent Kohn−Sham orbital ψ_i^{σ}. It is important to mention that a true dynamical spin-polarized exchange-correlation potential could better represent the transport properties in a molecular junction.[33,34] However, considering the complexity of the present problem in dealing with bias-dependent spin-polarized electronic current in a chemically bonded junction, ground-state-based DFT would be a good approximation.[22,35−39]

The next step is to create a non-equilibrium (NEB) situation, which refers to the bias condition, when the self-consistent potential drop at the lead on one side is different from that on the opposite side. The equilibrium situation refers to the condition when both leads are at the same potential. To establish this NEB situation, we have included an electric dipole interaction term as a perturbation in the Hamiltonian of the active scattering region.

$$H^{\sigma}(\varepsilon) = H^{\sigma}(0) + \vec{\varepsilon}\sum_i \vec{r}\,(i) \qquad (1)$$

where $H^{\sigma}(0)$ is the ground-state Hamiltonian in the absence of the electric field; $\vec{\varepsilon}$ is the applied dipole electric field along the axis parallel to the direction of the current, and $\vec{r}_i$ is the coordinate of the *i*th electron with spin σ; the charging effect on the DTB is considered by including a finite part of the electrode. Since the perturbed dipole interaction term contains only single-particle interaction, it can simply be added to the core Hamiltonian during the self-consistent calculation. Unlike the conventional perturbation approach, the self-consistent inclusion of the dipole interaction term into the core Hamiltonian allows us to include both first and higher order Stark effects in our calculation. This approach allows us to create charge surplus (source) and charge depletion (drain) at two metallic leads, resulting in a *local resistivity dipole*.[39]

A single-particle scattering formalism is used to calculate the current across the device, where the bias-dependent spin-polarized Green's function is calculated as

$$G^{\sigma}(E,\varepsilon) = [E \times S_{mm} - H_{mm}^{\sigma}(\varepsilon) - \Sigma_l^{\sigma}(\varepsilon) - \Sigma_r^{\sigma}(\varepsilon)]^{-1} \qquad (2)$$

$H_{mm}^{\sigma}(\varepsilon)$ is the bias-dependent Kohn−Sham molecular Hamiltonian obtained by suitable partitioning of $H^{\sigma}(\varepsilon)$. The use of the real-space approach for the *active* scattering region allows us to partition the $H^{\sigma}(\varepsilon)$ to obtain $H_{mm}^{\sigma}(\varepsilon)$. *E* is the injection energy of the tunneling electron, and S_{mm} is the molecular overlap matrix. $\Sigma_{l,r}^{\sigma}(\varepsilon)$ are the bias-dependent, spin-polarized self-energy functions, which are calculated as

$$\Sigma_{l,r}^{\sigma}(\varepsilon) = C_{l,r}^{\sigma\dagger}[g_{l,r}^{\sigma}(E)]_{n\times n}C^{\sigma}{}_{l,r} \qquad (3)$$

where $C_{l,r}^{\sigma}$ are the bias-dependent molecule-lead coupling matrices. These matrices are expressed as

$$C_l^{\sigma} = E \times S_{lm} - H_{lm}^{\sigma};\ C_r^{\sigma} = E \times S_{mr} - H_{mr}^{\sigma} \qquad (4)$$

$H_{lm}^{\sigma}(H_m^{\sigma})$ and $S_{lm}(S_{mr})$ are the electrode−molecule block of the Hamiltonian and overlap matrices on the left (right). This approach allows us to explicitly include the non-equilibrium nature of the interfacial electronic coupling into our model.[39] The $g_{l,r}^{\sigma}$ are the Green's functions of the leads. In the parallel configuration

$$g_l^{\sigma}(E) = -i\pi\eta^{\sigma}(E) \times I_n;\ g_l^{\sigma}(E) = g_r^{\sigma}(E) \qquad (5)$$

In the APC, for $\sigma = \uparrow$

$$g_r = -i\pi\eta^{\downarrow}(E) \times I_n;\ g_l = -i\pi\eta^{\uparrow}(E) \times I_n \qquad (6)$$

and for $\sigma = \downarrow$

$$g_r = -i\pi\eta^{\uparrow}(E) \times I_n;\ g_l = -i\pi\eta^{\downarrow}(E) \times I_n \qquad (7)$$

I_n is an identity matrix of dimension $n \times n$; *n* is the total number of Gaussian basis functions used to represent the Ni atoms in the active scattering part of the device. A periodic DFT is used to obtain $\eta^{\sigma}(E)$; it is calculated as DOS(*E*) per electron in the unit cell, where DOS(*E*) is the spin-polarized bulk (3D) density of states of nickel. For DOS(*E*), the energy grid is taken as 0.001 eV; the same energy grid is used for the integration in eq 8 to calculate the current. We have aligned the Fermi energy level of the active region of the device at the equilibrium condition with the Fermi energy of the bulk nickel. The Fermi energies of the active region for PC and APC are taken as the energies of their respective highest occupied molecular orbitals (HOMO). In case of PC and APC, we found that the HOMO corresponds to a spin-down state. It should be noted that the finite part of the Ni electrode on each side in the active scattering region and the respective unperturbed semi-infinite part of the electrode are assumed to have the same magnetic domain.

The current as a function of applied bias is calculated within coherent scattering approximation using the multichannel Landauer−Büttiker formalism.[23] The incoherent and spin-flip scattering effects are neglected as this molecular spacer consists of atoms with low atomic number, which lacks spin−orbit interactions. Hence, the total current can be written as a simple sum of spin-up and spin-down currents. Each component of current is calculated as

$$I_{\text{SD}}^{\sigma} = \frac{e}{h}\int_{\mu_1}^{\mu_2} T^{\sigma}(E,V) \times [f(E,\mu_2) - f(E,\mu_1)] \times \mathrm{d}E \qquad (8)$$

$T^{\sigma}(E,V)$ is the bias-dependent spin-polarized transmission function calculated as

$$T^{\sigma}(E,V) = Tr(\Gamma_l^{\sigma}G^{\sigma}\Gamma_r^{\sigma}G^{\sigma\dagger}) \qquad (9)$$

where $\Gamma^{\sigma}_{l,r} = i(\Sigma^{\sigma}_{l,r} - \Sigma^{\sigma\dagger}_{l,r})$ is the broadening function that determines the escape rate of the electron with spin σ.

In eq 8, e is the electronic charge, h is Planck's constant, and f is the Fermi distribution function; $\mu_{1,2}$ are calculated as

$$\mu_{1,2} = E_f \mp V_{low,\,high} \quad (10)$$

E_f is the equilibrium Fermi energy; V_{low} and V_{high} are the voltage drops at the electrodes, which are calculated self-consistently.[39−41]

The potential difference, V_{SD}, is obtained from the difference of V_{low} and V_{high}; at equilibrium, $V_{low} = V_{high} = 0$. We have also subtracted (added) a small thermal smearing term, k_BT (=0.026 eV) from (into) the lower (upper) limit of the integration in eq 8 to account for the electronic temperature at the interface in the non-equilibrium condition.

Conflict of Interest: The authors declare no competing financial interest.

Acknowledgment. We thank Samuel Trickey for helpful discussions during this work. This work is supported by NSF through Grant No. 0643420.

REFERENCES AND NOTES

1. Donhauser, Z. J.; Mantooth, B. A.; Kelly, K. F.; Bumm, L. A.; Monnell, J. D.; Stapleton, J. J.; Price, D. W., Jr.; Rawlett, A. M.; Allara, D. L.; Tour, J. M.; Weiss, P. S. Conductance Switching in Single Molecules through Conformational Changes. *Science* **2001**, *292*, 2303–2307.
2. Reed, M. A.; Zhou, C.; Muller, C. J.; Burgin, T. P.; Tour, J. M. Conductance of a Molecular Junction. *Science* **1997**, *278*, 252–254.
3. Xu, B.; Tao, N. J. Measurement of Single-Molecule Resistance by Repeated Formation of Molecular Junctions. *Science* **2003**, *301*, 1221–1223.
4. Zhou, J.; Chen, F.; Xu, B. Fabrication and Electronic Characterization of Single Molecular Junction Devices: A Comprehensive Approach. *J. Am. Chem. Soc.* **2009**, *131*, 10439–10446.
5. Hihath, J.; Bruot, C.; Nakamura, H.; Asai, Y.; Dez-Perez, I.; Lee, Y.; Yu, L.; Tao, N. Inelastic Transport and Low-Bias Rectification in a Single Molecule Diode. *ACS Nano* **2011**, *5*, 8331–8339.
6. Barraud, C.; Seneor, P.; Mattana, R.; Fusil, S.; Bouzehouane, K.; Deranlot, C.; Graziosi, P.; Hueso, L.; Bergenti, I.; Dediu, V.; *et al.* Unravelling the Role of the Interface for Spin Injection into Organic Semiconductors. *Nat. Phys.* **2010**, *6*, 615–620.
7. Schulz, L.; Nuccio, L.; Willis, M.; Desai, P.; Shakya, P.; Kreouzis, T.; Malik, V. K.; Bernhard, C.; Pratt, F. L.; Morley, N. A.; *et al.* Engineering Spin Propagation Across a Hybrid Organic/Inorganic Interface Using a Polar Layer. *Nat. Mater.* **2011**, *10*, 39–44.
8. Santos, T. S.; Lee, J. S.; Migdal, P.; Lekshmi, I. C.; Satpati, B.; Moodera, J. S. Room-Temperature Tunnel Magnetoresistance and Spin-Polarized Tunneling through an Organic Semiconductor Barrier. *Phys. Rev. Lett.* **2007**, *98*, 016601-4.
9. Xiong, Z. H.; Wu, Di; Vardeny, V.; Jing, S. Giant Magnetoresistance in Organic Spin-Valves. *Nature* **2004**, *427*, 821–824.
10. Majumdar, S.; Majumdar, H. S.; Laiho, R.; Osterbacka, R. Comparing Small Molecules and Polymer for Future Organic Spin-Valves. *J. Alloys Compd.* **2006**, *423*, 169–171.
11. Dediiu, V.; Hueso, L. E.; Bergenti, I.; Riminucci, A.; Borgatti1, F.; Graziosi, P.; Newby, C.; Casoli, F.; De Jong, M. P.; Taliani, C.; *et al.* Room-Temperature Spintronic Effects in Alq3-Based Hybrid Devices. *Phys. Rev. B* **2008**, *78*, 115203-6.
12. Lekshmi, I. C.; Buonsanti, R.; Nobile, C.; Rinaldi, R.; Cozzoli, P. D.; Maruccio, G. Tunneling Magnetoresistance with Sign Inversion in Junctions Based on Iron Oxide Nanocrystal Superlattice. *ACS Nano* **2011**, *5*, 1731–1738.
13. Sanvito, S. Molecular Spintronics: The Rise of Spinterface Science. *Nat. Phys.* **2010**, *6*, 562–564.
14. Sanvito, S. Molecular Spintronics. *Chem. Soc. Rev.* **2011**, *40*, 3336–3355.
15. Pati, R.; Senapati, L.; Ajayan, P. M.; Nayak, K. First Principles Calculations of Spin-Polarized Electron Transport in a Molecular Wire: Molecular Spin Valve. *Phys. Rev. B* **2003**, *68*, 100407(R)-4.
16. Waldron, D.; Haney, P.; Larade, B.; MacDonald, A.; Guo, H. Nonlinear Spin Current and Magnetoresistance of Molecular Tunnel Junctions. *Phys. Rev. Lett.* **2006**, *96*, 166804-4.
17. Ning, Z.; Zhu, Y.; Wang, J.; Guo, H. Quantitative Analysis of Nonequilibrium Spin Injection into Molecular Tunnel Junctions. *Phys. Rev. Lett.* **2008**, *100*, 056803-4.
18. Rocha, A. R.; Garcia-Suarez, V. M.; Bailey, S. W.; Lambert, C. J.; Ferrer, J.; Sanvito, S. Towards Molecular Spintronics. *Nat. Mater.* **2005**, *4*, 335–339.
19. Senapati, L.; Pati, R.; Erwin, S. C. Controlling Spin-Polarized Electron Transport through a Molecule: The Role of Molecular Conformation. *Phys. Rev. B* **2007**, *76*, 024438-5.
20. Dalgleish, H.; Kirczenow, G. Molecular Spintronics: Spin-Dependent Electron Transport in Molecular Wires. *Phys. Rev. B* **2005**, *72*, 184407-5.
21. Nitzan, A.; Ratner, M. A. Electron Transport in Molecular Wire Junctions. *Science* **2003**, *300*, 1384–1389.
22. Taylor, J.; Guo, H.; Wang, J. *Ab Initio* Modeling of Quantum Transport Properties of Molecular Electronic Devices. *Phys. Rev. B* **2001**, *63*, 245407-13.
23. Datta, S. *Electron Transport in Mesoscopic Systems*; Cambridge University Press: Cambridge, UK, 1997.
24. Di Ventra, M. *Electrical Transport in Nanoscale Systems*; Cambridge: New York, 2008.
25. Pati, R.; McClain, M.; Bandyopadhyay, A. Origin of Negative Differential Resistance in a Strongly Coupled Single Molecule−Metal Junction Device. *Phys. Rev. Lett.* **2008**, *100*, 246801-4.
26. Coey, J. M. D.; Venkatesan, M.; Fitzgerald, C. B.; Douvalis, A. P.; Sanders, I. S. Ferromagnetism of a Graphite Nodule from the Canyon Diablo Meteorite. *Nature* **2002**, *420*, 156–159.
27. Mertins, H.-Ch.; Valencia, S; Gudat, W.; Oppeneer, P. M.; Zaharko, O.; Grimmer, H. Direct Observation of Local Ferromagnetism on Carbon in C/Fe Multilayers. *Europhys. Lett.* **2004**, *66*, 743.
28. Atodiresei, N.; Brede, J.; Lazić, P.; Caciuc, V.; Hoffmann, G.; Wiesendanger, R.; Blügel, S. Design of the Local Spin Polarization at the Organic-Ferromagnetic Interface. *Phys. Rev. Lett.* **2010**, *105*, 066601-4.
29. Liu, D.; Hu, Y.; Guo, H.; Han, X. F. Magnetic Proximity Effect at the Molecular Scale: First-Principles Calculations. *Phys. Rev. B* **2008**, *78*, 193307-4.
30. *Gaussian 03*; Gaussian Inc.: Pittsburgh, PA, 2003.
31. Solomon, G. C.; Herrmann, C.; Vura-Weis, J.; Wasielewski, M. R.; Ratner, M. A. The Chameleonic Nature of Electron Transport through π-Stacked Systems. *J. Am. Chem. Soc.* **2010**, *132*, 7887–7889.
32. Ruden, P. Organic Spintronics: Interfaces are Critical. *Nat. Mater.* **2011**, *10*, 8–9.
33. Runge, E.; Gross, E. K. U. Density-Functional Theory for Time-Dependent Systems. *Phys. Rev. Lett.* **1984**, *52*, 997–1000.
34. Sai, N.; Zwolak, M.; Vignale, G.; Di Ventra, M. Dynamical Corrections to the DFT-LDA Electron Conductance in Nanoscale Systems. *Phys. Rev. Lett.* **2005**, *94*, 186810-4.
35. Brandbyge, M.; Mozos, J. L.; Ordejon, P.; Taylor, J.; Stokbro, K. Density-Functional Method for Nonequilibrium Electron Transport. *Phys. Rev. B* **2002**, *65*, 165401-17.
36. Xue, Y.; Datta, S.; Ratner, M. A. Charge Transfer and "Band Lineup" in Molecular Electronic Devices: A Chemical and Numerical Interpretation. *J. Chem. Phys.* **2001**, *115*, 4292–4299.
37. Su, W.; Jiang, J.; Lu, W.; Luo, Y. First-Principles Study of Electrochemical Gate-Controlled Conductance in Molecular Junctions. *Nano Lett.* **2006**, *6*, 2091–2094.
38. Solomon, G. C.; Herrmann, C.; Hansen, T.; Mujica, V.; Ratner, M. A. Exploring Local Currents in Molecular Junctions. *Nat. Chem.* **2010**, *2*, 223–228.
39. Mandal, S.; Pati, R. Mechanism Behind the Switching of Current Induced by a Gate Field in a Semiconducting Nanowire Junction. *Phys. Rev. B* **2011**, *84*, 115306-5.

40. Mandal, S.; Pati, R. Codoping in a Single Molecular Junction from First Principles. *Phys. Rev. B* **2011**, *83*, 195420-9.
41. Pal, P. P.; Pati, R. First-Principles Study of the Variation of Electron Transport in a Single Molecular Junction with the Length of the Molecular Wire. *Phys. Rev. B* **2010**, *82*, 045424-6.